Characterization of a chiral phase in an achiral bent-core liquid crystal by polarization studies of resonant x-ray forbidden reflections

V. Ponsinet,[1] P. Barois,[1] LiDong Pan,[2] Shun Wang,[2] C. C. Huang,[2] S. T. Wang,[3] R. Pindak,[3] U. Baumeister,[4] and W. Weissflog[4]

[1]*Centre de Recherche Paul Pascal, Université Bordeaux 1, CNRS, Av. A. Schweitzer, FR-33600 Pessac, France*

[2]*School of Physics and Astronomy, University of Minnesota, Minneapolis, Minnesota 55455, USA*

[3]*Brookhaven National Laboratory, National Synchrotron Light Source, Upton, New York 11973, USA*

[4]*Martin-Luther-Universität Halle-Wittenberg, Institut für Chemie, DE-06120 Halle, Germany*

(Received 13 April 2011; published 15 July 2011)

The chiral antiferroelectric structure of an achiral bent-core liquid crystal is characterized by resonant x-ray scattering at chlorine *K* edge. The "forbidden" reflections resulting from the glide or screw symmetry elements are restored by the anisotropy of the tensor structure factor, which we calculate for two possible structural models. A careful analysis of the polarization states of the restored "forbidden" reflections enables an unambiguous identification of a chiral structure (i.e., the so-called anticlinic, antiferroelectric smectic-*C* or Sm-$C_A P_A$) coexisting with the achiral synclinic antiferroelectric smectic-*C* or Sm-$C_S P_A$. The method proves to be quite powerful as it identifies the chiral structure within coexisting phases despite an imperfect orientation of the sample. The volume fraction of the chiral phase and the distribution of alignment are extracted from the data.

DOI: 10.1103/PhysRevE.84.011706 PACS number(s): 61.30.Eb, 61.05.C−

Thermotropic liquid crystals (LCs) are complex fluids resulting from low-dimensional self-organization of organic molecules of specific architecture (mesogens) generally constituted of a rigid core (imposing the global shape) surrounded by or terminated by flexible chains. The most common shapes of mesogens are rods and disks. In recent years, LCs made of bent-core molecules have attracted a lot of attention for their rich and complex polymorphism, and for unexpected physical properties such as ferroelectricity or the presence of twisted structures in achiral materials [1–3]. Unlike rodlike or disklike mesogens, the description of the orientation of a bent-core molecule requires two vector fields [3], namely, the string **n** and the arrow **b** in the convenient picture of a bow. The phases resulting from the spatial organization of these two fields have been assigned names B_1 to B_7 as they were discovered [4]. Among them, the so-called B_2 phase shows a lamellar structure formed by a regular stack of liquid layers of thickness d along a direction Z. Four microscopic models have been proposed [Fig. 1] that correspond to the four combinations of the Sm-*C*-like tilt of the string (synclinic or anticlinic) and of the polarization borne by the arrow (ferroelectric or antiferroelectric). The general notation Sm-$C_{S\,\mathrm{or}\,A} P_{F\,\mathrm{or}\,A}$ summarizes these four states. The in-plane axes X (along the tilt direction) and Y (along the arrow) complete the reference frame. Link *et al.* [5] have pointed out that the individual layers of the proposed structures are chiral (i.e., different from their mirror image) although the molecules are achiral. Two of the proposed structures are also chiral (namely, Sm-$C_S P_F$ and Sm-$C_A P_A$), whereas Sm-$C_S P_A$ and Sm-$C_A P_F$ are racemic stacks of layers of opposite handedness.

From a crystallographic point of view, the unit cell is one layer for the Sm-$C_S P_F$ structure, but two layers of opposite tilt and/or polarization for the other three. In reciprocal space, the basic wave vector component Q_Z of the latter is then $Q_0/2$, with $Q_0 = 2\pi/d$. The half-order Bragg reflections (in Q_0 units) are forbidden by the classical extinction rules [i.e., glide plane *(X,Z)* for the Sm-$C_S P_A$ phase, glide plane *(Y,Z)* for Sm-$C_A P_F$, and 2_1 screw axis for Sm-$C_A P_A$], which implies that the four structures can not be distinguished by conventional diffraction of x rays.

It was shown in a previous work [6] that resonant x-ray diffraction (RXRD) could be used to overcome this problem. Indeed, the half-order forbidden reflections were observed (hence, ruling out the Sm-$C_S P_F$ phase) and a careful analysis of their polarization state enabled the unambiguous characterization of the Sm-$C_S P_A$ phase.

However, electro-optical studies of various B_2 phases found in other materials claimed that different structures may exist, depending on the electrical history of a sample [4]. Reports by Barnik *et al.* [7] on the possible coexistence of two antiferroelectric B_2 phases in a bent-core material were particularly intriguing. The coexistence of two phases over an extended temperature range in a pure compound is, in principle, forbidden by the phase rule. It may, however, occur in thin films if the interaction with the surfaces stabilizes a second phase or if metastable states are trapped by slow kinetics. This paper is devoted to a structural characterization by resonant scattering of the bent-core material studied in Ref. [7]. The aim of our study is to characterize unambiguously the reported Sm-$C_A P_A$ structure and determine whether it appears in a pure phase or in coexisting phases.

The bent-core liquid crystal studied is the homolog ($n = 14$) of the series 4-chloro-1,3-phenylene bis[4-(4-*n*-alkylphenyliminomethyl) benzoate] [8] (or 14 PBCl for short). The molecular structure is given in Fig. 2. The two-layer superstructure of the B_2 phase of this material was first confirmed by resonant scattering [9]. The Sm-*C*-like tilt angle α was measured independently by conventional x-ray scattering on oriented samples yielding an experimental value of $28^\circ \pm 3^\circ$. Electro-optical studies of this material [10] exhibited an antiferroelectric response, but optical observations showed the presence of circular domains rotating in opposite directions under field, hence revealing the presence of chiral domains of opposite handedness. This observation, not consistent with

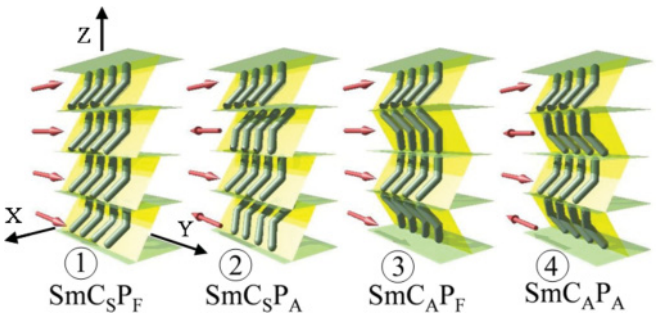

FIG. 1. (Color online) Sketch of the four possible structures of the B_2 phase. The arrows show the polarization within each layer. The unit cell is two layers for structures 2, 3, and 4.

the achiral Sm-C_SP_A structure, suggests a Sm-C_AP_A phase instead.

I. THEORETICAL BACKGROUND

The technique of resonant scattering was successfully applied to resolve the structure of chiral [11,12] and bent-core [6] liquid crystals. Let us recall briefly that resonant (or anomalous) x-ray scattering occurs when the energy of the x-ray radiation approaches the values required to excite an inner-shell electron into an empty state of the outer shell [13]. In such circumstances, the atomic scattering factor fa exhibits a complex frequency-dependent contribution in addition to the classical (nonresonant) term f_0, which is the Fourier transform of the electron density. The resonant contribution depends on the atom and becomes substantial near its absorption edges. Because of the local anisotropy of the outer-shell unoccupied states, the resonant structure factor is a tensor that reflects the symmetry of the resonant atom within the molecule. The anisotropy of this tensor leads to the observation of forbidden reflections and determines their nontrivial polarization properties. The variations of the polarization state and of the intensity of the resonant forbidden reflections have been worked out by Dmitrienko as a function

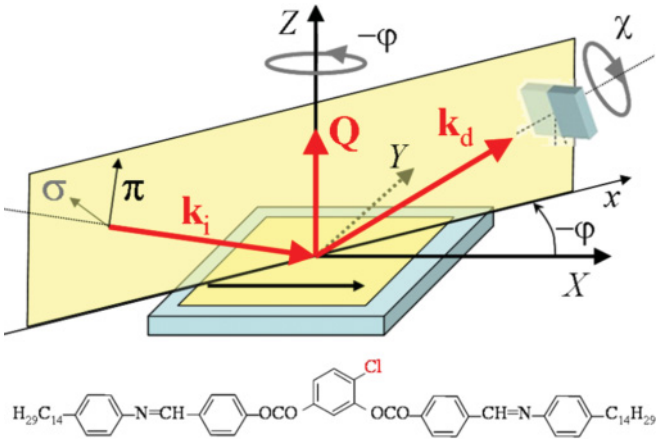

FIG. 2. (Color online) Top: experimental scattering geometry. The $\boldsymbol{\pi}$ component of the polarization of the incident x-ray beam is null. The polarization of the diffracted beam is analyzed by a pyrolytic (002) graphite crystal. The black arrow on sample denotes the direction of shear of the liquid crystal film. Bottom: chemical formula of the 14PBCl liquid crystal.

of the rotation angle φ of the sample about the scattering vector **Q** for cubic crystals in kinematic theory [14]. This theoretical work was used in Ref. [6] to characterize the Sm-C_SP_A structure. Let us recall how it applies to the structures of the B_2 phases.

The structure factor tensor was derived in each phase from the basic symmetries of the molecule and of the unit cell. For the half-order forbidden reflections of the two antiferroelectric phases, the tensors have the form [6]

$$\tilde{\tilde{F}}(\text{Sm-}C_SP_A) = \begin{bmatrix} 0 & iA\sin\alpha & 0 \\ iA\sin\alpha & 0 & iA\cos\alpha \\ 0 & iA\cos\alpha & 0 \end{bmatrix}, \quad \text{(1a)}$$

$$\tilde{\tilde{F}}(\text{Sm-}C_AP_A) = \begin{bmatrix} 0 & 0 & B\sin 2\alpha \\ 0 & 0 & iA\cos\alpha \\ B\sin 2\alpha & iA\cos\alpha & 0 \end{bmatrix}. \quad \text{(1b)}$$

A and B are unknown complex numbers and α is the tilt angle of the string with respect of the axis Z (layer normal). The scattering amplitudes $\bar{A}_{\gamma\delta}$ derive simply from the tensors via the usual formulas [14]

$$\bar{\mathbf{A}}_{\boldsymbol{\gamma}\boldsymbol{\delta}} = \boldsymbol{\gamma} \cdot \tilde{\tilde{\mathbf{F}}}\,\boldsymbol{\delta} \quad (2)$$

in which the incident and diffracted polarization vectors $\boldsymbol{\delta}$ and $\boldsymbol{\gamma}$ can take the two values $\boldsymbol{\pi}$ (in the scattering plane) or $\boldsymbol{\sigma}$ (perpendicular to the scattering plane). The scattering geometry is shown in Fig. 2. In our experiment, the incident beam is $\boldsymbol{\sigma}$ polarized so that the incident $\boldsymbol{\pi}$ polarization is not considered.

The polarization state of the resonant Bragg peaks, hence, depends on the orientation φ of the sample [14]. The general form of the scattered intensity can be expressed as [6]

$$\begin{aligned} I(\varphi,\chi)/A^2\sin^2\alpha &= a_\sigma^2\cos^2\chi + a_\pi^2\sin^2\chi + 2a_\sigma a_\pi\sin\chi\cos\chi \\ &= \left(a_\sigma^2 + a_\pi^2\right)\cos^2(\chi-\omega) \end{aligned} \quad (3)$$

with $a_\sigma = -\bar{A}_{\sigma\sigma}/iA\sin\alpha$, $a_\pi = -\bar{A}_{\sigma\pi}/iA\sin\alpha$, and $\omega = \arctan(a_\pi/a_\sigma)$.

In the Sm-C_SP_A phase, the rescaled coefficients are both real: $a_\sigma = a_{S,\sigma} = \sin 2\varphi$ and $a_\pi = a_{S,\pi} = (\sin\theta_B\cos 2\varphi - \cos\theta_B\cos\varphi/\tan\alpha)$. In the Sm-$C_AP_A$ phase, $a_{A,\sigma} = 0$ and $a_{A,\pi} = -\cos\theta_B\cos\varphi/\tan\alpha - 2iB/A\cos\alpha\cos\theta_B\sin\varphi$. Here, θ_B is the Bragg angle of the resonant peak chosen at $Q_z = 3/2\ Q_0$ to avoid the strong reflected background at $1/2Q_0$.

The polarization of the resonant peaks is hence linear and rotated by an angle ω with respect to the polarization direction of the incident x rays in the two antiferroelectric phases of interest, namely, Sm-C_SP_A and Sm-C_AP_A:

$$\begin{aligned} \omega(\varphi) &= \arctan[(\sin\theta_B\cos 2\varphi - \cos\theta_B\cos\varphi/\tan\alpha)/\sin 2\varphi] \\ &\qquad\qquad \text{for Sm-}C_SP_A \\ \text{and} \quad \omega(\varphi) &= \pi/2 \quad \text{for Sm-}C_AP_A \end{aligned} \quad (4)$$

The expected variations $\omega(\varphi)$ are plotted in Fig. 3.

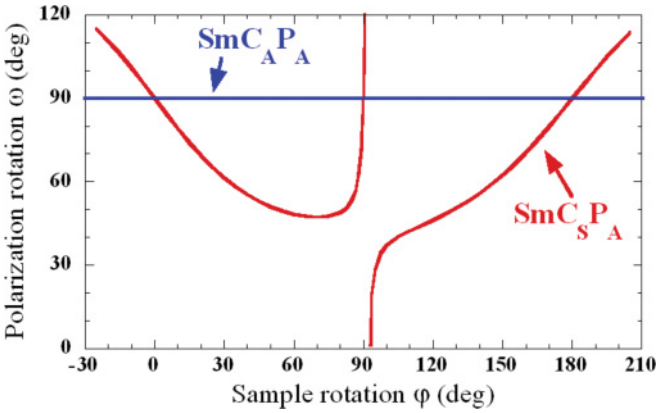

FIG. 3. (Color online) Rotation ω of the polarization vs rotation φ of the sample calculated for the two antiferroelectric B_2 phases. The Sm-$C_S P_A$ curve is calculated with Eq. (4) for the true experimental values of the Bragg angle of the 3/2 resonant reflection $\theta_B = 4.07^\circ$ and of the tilt angle $\alpha = 28^\circ$ with no adjustable parameter.

II. EXPERIMENTS

The experimental conditions are similar to those described in Ref. [6]. The bent-core LC material 14PBCl exhibits the following phase sequence on cooling: transition from Isotropic to B2 (at $T = 127\,^\circ$C) and transition from B2 to crystal (at $T = 68\,^\circ$C) [8]. It was spread in the B_2 phase by shearing a drop of the material along one direction on a 12 × 12 mm^2 glass substrate treated by deposition of a thin layer of surfactant (hexadecyl trimethyl ammonium bromide). The x-ray experiments were carried out at beamline X-19A of the National Synchrotron Light Source. A complete description of the three-circle diffraction setup was given in an earlier paper [12]. The LC sample was mounted on an additional motorized φ rotation stage around the Z axis fitted inside a two-stage oven allowing 20 mK resolution in temperature.

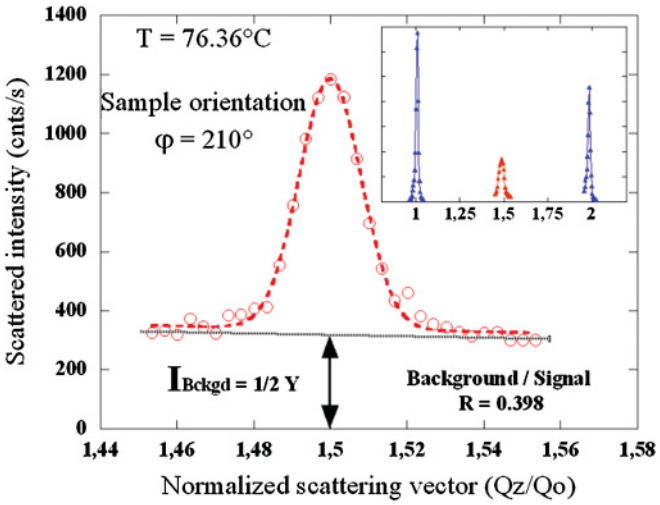

FIG. 4. (Color online) Normalized Q_z scan across the 3/2 resonant peak without polarizer crystal at chlorine K edge. The dashed line is a fit to a Gaussian profile superimposed on a slowly decaying background. Inset shows a wider scan displaying the nonresonant (001) ($\times 10^{-5}$) and (002) ($\times 1/25$) Bragg peaks.

The polarization of the diffracted beam could be analyzed by a pyrolytic graphite crystal mounted on the two-theta arm. The beam size was set to 200 (vertical) × 500 (horizontal) μm^2, and the ΔQ_z resolution was 1.9×10^{-3} Å^{-1}. A fluorescence energy scan was first performed to tune the energy to the chlorine K edge at 2.823 keV.

The x-ray diffraction experiments were performed at $T = 76.36\,^\circ$C in the B_2 phase. The forbidden Bragg reflexion at $Q_z = 3/2\ Q_0$ was first recorded without the analyzer crystal. In this geometry, both components $\boldsymbol{\sigma}$ and $\boldsymbol{\pi}$ of the diffracted beams are collected. Figure 4 shows a typical scan of the intensity scattered along the direction Q_z perpendicular to the smectic layers. It shows a sharp resonant 3/2 reflexion superimposed on a background scattering that slowly decays with Q_z. This nonresonant background is mainly due to the reflectivity of the air-liquid crystal interface and may contain contributions from the Kapton windows and helium gas in the flight path. The layer thickness d was 46.9 Å. Transverse θ scans across the Bragg peaks showed that the alignment of the layers was better than 0.02°.

The polarization of the Bragg peaks was then recorded by rotating the polarimeter about the direction $\mathbf{k}_d$ of the diffracted beam. The rotation axis of the polarimeter was first carefully aligned along $\mathbf{k}_d$ through a couple of 0.5-mm pinhole apertures. In order to avoid a possible mechanical bias, a rocking scan of the graphite crystal was performed for each value of the polarimeter angle χ.

The linear $\boldsymbol{\sigma}$ polarization of the incident synchrotron beam and of the nonresonant (001) and (002) Bragg peaks were checked first, defining the origin of the polarimeter angle $\chi = 0$ on a maximum of intensity. The extinction was almost complete (residual intensity was about 1.5%–3.5% of the maximum intensity) and consistent with the less than optimal Bragg angle $\theta_{B\ \mathrm{Crystal}} = 41.05^\circ$ of the graphite crystal.

The polarization of the 3/2 resonant peak was then investigated for different values of φ. Figure 5 shows, for example, the intensity of the resonant signal versus rotation χ of the analyzer crystal for the same sample position as in

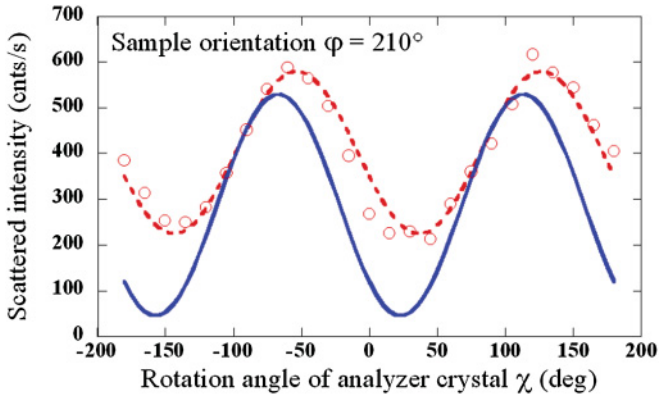

FIG. 5. (Color online) Polarimeter scan $I(\varphi = 210^\circ, \chi)$ recorded on the resonant peak shown in Fig. 4. The data points (open circles) are fitted to Eq. (5) (dashed line). The solid line shows the corrected function after subtraction of the σ-polarized background and less than optimal analyzer angle correction [Eq. (9)]. The residual value of the minima is due to the imperfect in-plane orientation of the sample.

Fig. 4, $\varphi = 210°$. For each value of φ, the experimental signal can be fitted to the following function:

$$I_{\mathrm{expt}}(\varphi,\chi) = A2_m \cos^2\chi + B2_m \sin^2\chi + 2C_m \sin\chi\cos\chi. \tag{5}$$

This expression can not be simply identified with Eq. (3) since the experimental values of $A2_m$, $B2_m$, and C_m do not satisfy the condition ${C_m}^2 = A2_m B2_m$ and the data must be corrected for background contributions.

First of all, the $\boldsymbol{\sigma}$-polarized background appearing in Q_z scans (Fig. 4) contributes a term $Y(\varphi)\cos^2\chi$ to the scattering. Adding this term to Eq. (3) and averaging over χ yields the intensity recorded without analyzer crystal:

$$I^{\mathrm{No\ crystal}}(\varphi) = \left(a_\sigma^2 + a_\pi^2\right)/2 + Y/2. \tag{6}$$

The background-to-signal ratio R extracted from the experimental Q_z scan is then

$$R = Y/\left(a_\sigma^2 + a_\pi^2\right). \tag{7}$$

A weaker correction arises from the less than optimal analyzer crystal angle, which transmits a factor $\cos^2(2\theta_{B\ \mathrm{Crystal}}) = 0.024$ of the polarization orthogonal to its main axis. This contributes a term $\cos^2(2\theta_{B\ \mathrm{Crystal}})\ ({a_\sigma}^2\cos^2\boldsymbol{\chi} + {a_\pi}^2\sin^2\boldsymbol{\chi} - 2a_\sigma a_\pi \sin\chi\cos\chi)$ to the scattering in Eq. (3).

Subtracting these two contributions from Eq. (5) yields the new parameters $A2, B2$, and C corrected for background scattering and analyzer crystal Bragg angle:

$$A2 = \frac{A2_m[1+R\cos^2(2\boldsymbol{\theta}_{B\,\mathrm{Crystal}})] - B2_m[\cos^2(2\boldsymbol{\theta}_{B\,\mathrm{Crystal}})+R]}{(1+R)\sin^2(2\boldsymbol{\theta}_{B\,\mathrm{Crystal}})},$$

$$B2 = \frac{B2_m - A2_m\cos^2(2\boldsymbol{\theta}_{B\,\mathrm{Cryst}})}{\sin^2(2\boldsymbol{\theta}_{B\,\mathrm{Crystal}})}, \tag{8}$$

$$C = \frac{C_m}{\sin^2(2\theta_{B\,\mathrm{Crystal}})}.$$

Finally, the imperfection of the in-plane alignment of the sample must be accounted for. The most general case can be described by a distribution function $\mathcal{P}(\varphi')$ that measures the density of probability of a local in-plane orientation of the tilt at an angle φ' away from the direction of shear. The unknown function $\mathcal{P}$ is expected to be even and have a maximum at $\varphi' = 0$ by symmetry. Convoluting this function with Eq. (3) yields the intensity scattered by an imperfectly aligned phase

$$\langle I(\varphi,\chi)\rangle = A2\cos^2\chi + B2\sin^2\chi + 2C\sin\chi\cos\chi \tag{9}$$

with

$$A2(\varphi) = \int_{-\pi}^{\pi} d\varphi' \mathcal{P}(\varphi') a_\sigma^2(\varphi-\varphi'),$$

$$B2(\varphi) = \int_{-\pi}^{\pi} d\varphi' \mathcal{P}(\varphi') a_\pi^2(\varphi-\varphi'), \tag{10}$$

$$C(\varphi) = \int_{-\pi}^{\pi} d\varphi' \mathcal{P}(\varphi') a_\sigma(\varphi-\varphi') a_\pi(\varphi-\varphi').$$

Equations (8)–(10) hence yield the wanted relationship between the measured parameters $A2_m$, $B2_m$, and C_m and the theoretical formulas [Eq. (3)]. The experimental orientation

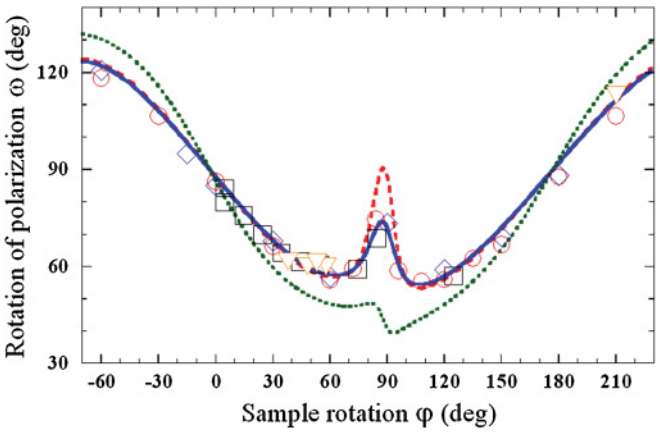

FIG. 6. (Color online) Experimental rotation of the polarization of the 3/2 resonant Bragg peak ω_{expt} vs sample rotation φ. Different symbols correspond to different samples of the same material. The dashed and solid lines are the best fits to the model of coexisting Sm-$C_S P_A$ and Sm-$C_A P_A$ phases with perfect in-plane alignment (dashed) and with a Gaussian distribution of in-plane orientation of width $15 \pm 1°$ (solid) for $p = 0.118 \pm 0.002$, $q = 1.80 \pm 0.01$, and $r = 0.026 \pm 0.002$. The dotted line is the polarization calculated for the pure Sm-$C_S P_A$ phase with the same distribution of in-plane orientation and no other free parameter.

ω_{expt} of the polarization corresponds to the maxima of Eq. (9). Simple trigonometric algebra yields

$$\tan\omega_{\mathrm{expt}} = \mathrm{sgn}(C)|b/a| \tag{11}$$

with

$$a^2 = (A2 - B2 + \sqrt{(A2-B2)^2 + 4C^2})/2$$

and

$$b^2 = (B2 - A2 + \sqrt{(A2-B2)^2 + 4C^2})/2.$$

The rotation ω_{expt} of the polarization is plotted in Fig. 6 versus φ. The strong variation of ω_{expt} with φ clearly rules out the pure Sm-$C_A P_A$ model (i.e., $\omega_{\mathrm{expt}} = 90°$ for all φ). Moreover, we found that the experimental data could not be fitted to the Sm-$C_S P_A$ model with any possible width and shape of the distribution function $\mathcal{P}$ (φ'). As an illustration, the dotted line in Fig. 6 is calculated from Eqs. (9) and (10) with a Gaussian function $\mathcal{P}$ (φ') of width 15° [full width at half maximum (FWHM)].

We then tried to fit our data to a model of coexisting Sm-$C_S P_A$ and Sm-$C_A P_A$ phases. In such a case, the theoretical intensity of resonant scattering follows from Eq. (3):

$$I_{\mathrm{mix}}(\varphi,\chi) = (1-f_{\mathrm{Vol}})a_{S,\sigma}^2\cos^2\chi + \left[(1-f_{\mathrm{Vol}})a_{S,\pi}^2 + f_{\mathrm{Vol}}|a_{A,\pi}|^2\right]\sin^2\chi + 2(1-f_{\mathrm{Vol}})a_{S,\sigma}a_{S,\pi}\sin\chi\cos\chi, \tag{12}$$

in which f_{Vol} is the volume fraction of the Sm-$C_A P_A$ phase in the mixture. We assume that the typical size of the Sm-$C_S P_A$ and Sm-$C_A P_A$ regions is larger than the coherence length $\xi \sim 300$ nm of the x-ray beam, so that intensities rather than amplitudes are added.

The π-polarized contribution of the Sm-$C_A P_A$ phase can be rewritten as

$$f_{\mathrm{Vol}}/(1-f_{\mathrm{Vol}})|a_{A,\pi}|^2 = p\,\sin^2\varphi + q\,\cos^2\varphi + 2r\sin\varphi\cos\varphi \qquad (13)$$

with

$$p = f_{\mathrm{Vol}}/(1-f_{\mathrm{Vol}})\,\eta^2\cos^2\alpha\,\cos^2\theta_B \qquad (14a)$$

$$q = f_{\mathrm{Vol}}/(1-f_{\mathrm{Vol}})\,\cos^2\theta_B/\tan^2\alpha \qquad (14b)$$

$$r = f_{\mathrm{Vol}}/(1-f_{\mathrm{Vol}})\,\eta\cos\psi\cos^2\theta_B\cos^2\alpha/\sin\alpha, \qquad (14c)$$

in which η and ψ are the modulus and phase of the unknown complex factor $2iB/A = \eta\exp(i\psi)$.

Figure 6 shows a fit of the experimental data to this model. The dashed line is calculated for a perfectly oriented sample. The solid line is the best fit obtained with a Gaussian distribution of the in-plane orientation of width $15 \pm 1^\circ$ (FWHM), $p = 0.118 \pm 0.002$, $q = 1.80 \pm 0.01$, and $r = 0.026 \pm 0.002$. Figure 6 clearly shows that the model of coexisting Sm-$C_S P_A$ and Sm-$C_A P_A$ phases is fully consistent with the experimental data. We checked that the quality of the fit is not sensitive to the exact profile of the distribution function (i.e., Gaussian or simple gate function gives similar results).

The volume fraction of the Sm-$C_A P_A$ phase can be estimated from Eq. (14b), which yields $f_{\mathrm{Vol}} = 34 \pm 6\%$. The large uncertainty is mostly due to the error bar on the value of the tilt angle $\alpha = 28^\circ \pm 3^\circ$.

In conclusion, this paper provides direct evidence of the existence of the chiral Sm-$C_A P_A$ structure in the B_2 phase of the 14PBCl material. We confirm that it coexists with the nonchiral Sm-$C_S P_A$ phase, in agreement with electro-optical studies of Barnik *et al.* [7]. The observation of the coexistence in two different geometries (closed cell in [7] and free surface in this paper) confirms that the two phases have very similar free energies; it is actually impossible to tell which of them corresponds to the ground state.

ACKNOWLEDGMENTS

Research at the NSLS, BNL, was supported in part by the US Department of Energy, Division of Materials Sciences and Division of Chemical Sciences, under Contract No. DE-AC02-98Ch-0886. The research was supported in part by the National Science Foundation, Solid State Program, under Grant No. DMR-0605760. V.P. acknowledges financial support from CNano-GSO for experiments at NSLS.

[1] T. Niori, T. Sekine, J. Watanabe, T. Furukawa, and H. Takezoe, J. Mater. Chem. **6**, 1231 (1996).
[2] G. Pelzl, S. Diele, and W. Weissflog, Adv. Mater. (Weinheim, Ger.) **11**, 707 (1999).
[3] H. R. Brand, P. E. Cladis, and H. Pleiner, Eur. Phys. J. B. **6**, 347 (1998).
[4] R. A. Reddy and C. Tschierske, J. Mater. Chem. **16**, 907 (2006).
[5] D. R. Link, G. Natale, R. Shao, J. E. Maclennan, N. A. Clark, E. Korblova, and D. M. Walba, Science **278**, 1924 (1997).
[6] P. Fernandes, P. Barois, S. T. Wang, Z. Q. Liu, B. K. McCoy, C. C. Huang, R. Pindak, W. Caliebe, and H. T. Nguyen, Phys. Rev. Lett. **99**, 227801 (2007).
[7] M. I. Barnik, L. M. Blinov, N. M. Shtykov, S. P. Palto, G. Pelzl, and W. Weissflog, Liq. Cryst. **29**, 597 (2002).
[8] W. Weissflog, C. Lischka, S. Diele, G. Pelzl, and I. Wirth, Mol. Cryst. Liq. Cryst. **328**, 101 (1999).
[9] A. Cady, R. Pindak, W. Caliebe, P. Barois, W. Weissflog, H. T. Nguyen, and C. C. Huang, Liq. Cryst. **29**, 1101 (2002).
[10] L. M. Blinov, M. I. Barnik, E. S. Bustamante, G. Pelzl, and W. Weissflog, Phys. Rev. E **67**, 021706 (2003).
[11] P. Mach, R. Pindak, A. M. Levelut, P. Barois, H. T. Nguyen, C. C. Huang, and L. Furenlid, Phys. Rev. Lett. **81**, 1015 (1998).
[12] P. Mach, R. Pindak, A. M. Levelut, P. Barois, H. T. Nguyen, H. Baltes, M. Hird, K. Toyne, A. Seed, J. W. Goodby, C. C. Huang, and L. Furenlid, Phys. Rev. E **60**, 6793 (1999).
[13] J. L. Hodeau, V. Favre-Nicolin, S. Bos, H. Renevier, E. Lorenzo, and J. F. Berar, Chem. Rev. **101**, 1843 (2001).
[14] V. E. Dmitrienko, Acta Crystallogr., Sect. A **39**, 29 (1983).